RASĀYAN *J. Chem.*
Vol. 15 | No. 4 |2466-2476| October - December | 2022
ISSN: 0974-1496 | e-ISSN: 0976-0083 | CODEN: RJCABP
http://www.rasayanjournal.com
http://www.rasayanjournal.co.in

MAGNETIC Fe_3O_4-CuO/BIOCHAR NANOCOMPOSITE FOR ADSORPTION OF INORGANIC ANIONS FROM AQUEOUS SOLUTION

A. Allwar[1,✉], R. Ahdiaty[1] and R. Doong[2]
[1]Department of Chemistry, Faculty of Mathematics and Natural Sciences
Universitas Islam Indonesia, Yogyakarta, Indonesia, 55584.
[2]The Institute of Analytical and Environmental Science, National Tsing Hua University, 101 Section 2, Kuang Fu Road, Hsinchu, Taiwan,30013.
✉Corresponding Author: allwar@uii.ac.id

ABSTRACT

In this study, biochar from palm oil shell waste was applied as supporting material for the immobilized iron and copper oxide to fabricate the magnetic adsorbent of Fe_3O_4-CuO/biochar. The characterization showed that metallic oxide Fe_3O_4 and CuO are dispersed on the surface of biochar with high accessibility. BET surface area is 263 m^2 g^{-1} relating to a predominantly microporous structure. FTIR spectra showed that the bands at 615.27 and 590.15 cm^{-1} are assigned to Cu-O-C and Fe-O-C stretching vibration, respectively. The average crystallized size for Fe_3O_4-CuO/biochar is 25 nm related to nanoparticle size. The efficiency of the adsorbent was observed from the percentage removal of inorganic anions in an aqueous solution. The highest efficiency of the adsorption process is found in the removal of phosphate at different pH solutions and contact times. The adsorption isotherms are matched for Langmuir and Freundlich models except for the fluoride. The kinetic model shows that pseudo-second-order is more favorable for the removal of inorganic anions than pseudo-first-order. This result indicated that Fe_3O_4-CuO/biochar is a promising adsorbent and will be effectively used for the removal of anions from an aqueous solution.

Keywords: Palm Oil Shell, Magnetic Fe_3O_4-CuO/biochar, Inorganic Anions, Adsorption, Crystallized Size.
RASĀYAN*J. Chem.*, Vol. 15, No.4, 2022

INTRODUCTION

Water and sanitation are natural sources that are vital requirements for human life and daily activities, including agriculture, fishery, animal husbandry, industry, and mining. The main problem is the decreasing quantity and quality of water supply. Recently, aquatic environment such as surface water, sea, and groundwater has been under stress due to human activities. Most chemical pollutants such as heavy metals, organic, and inorganic anions are from industrial and municipal activities that are the major source of water problem.[1, 2] The discharge of inorganic anion pollutants such as phosphate, nitrate, nitrite, and fluoride into the waterway has disturbed the ecological balance of micro-organism in the water. Phosphate and nitrate are usually used as supporting nutrients for the growth of plants and microorganisms.[3] However, at a high concentration in water, phosphate, and nitrate can cause serious problems to algae, fish, and other aquatic life.[4-6] A high level of nitrate in the drinking water can cause a stomach ache and carcinogen effects. The recovery of any type of anion pollutants in water resources is necessary to reduce serious environmental problems. This affords is likely the greatest challenge in the past ten years. Many researchers have proposed several methods to deal with these problems. Several technologies have been applied to remove any type of pollutants from water resources such as adsorption, precipitation, electrochemistry, and ion exchange. One of the most popular methods is the adsorption process.[7] Adsorption is widely used for the separation and purification process due to its simplicity, low-cost operational, and effective method.[8] The most common materials used for the adsorption process is the rich-carbon material with high pore structures. Biochar is well known porous material as an excellent adsorbent due to its high surface area, large pore volume, pore size distribution, various functional groups, and availability in large quantities. Previous work reported that the improvement of biochar properties is required to increase the adsorption capacity mainly for the removal of pollutants in the aqueous solution.[9] The incorporation of metal oxide with porous

http://doi.org/10.31788/RJC.2022.1547063

materials such as activated carbon, biochar, and zeolite has been promising to improve the adsorption capacity.[10] The nanocomposite of magnetic Fe_3O_4/biochar has shown a highly active site and is successfully used for the removal of dyes in water solution. Cu-supporting biochar has been used as a photocatalytic process for the degradation of p-nitrophenol showing good thermal conductivity and low friction coefficient.[11-13] In addition, Fe_3O_4-CuO supported with biochar is also applied as an adsorbent for the removal of dyes from an aqueous solution.[14] The magnetic metal oxide such as Fe_3O_4 supported with biochar has attracted attention as a suitable alternative adsorbent to remove the inorganic anions in the aqueous solution. The magnetic metal oxide may initiate to agglomeration of particles leading to reduce capacity and selectivity. However, to advance the applicability of metal oxide, it is necessary to combine metal oxide and porous material such as biochar. The function of metallic oxide can support enriching the surface chemistry of the adsorbent through the binding of metal-Oxygen on the surface of biochar.[15] Therefore, the incorporation of Fe_3O_4, CuO, and biochar as adsorbents is necessary to improve the adsorptive capacity in the removal of inorganic ions in an aqueous solution. Biochar is well known porous solid material and high functional groups that can bind metal oxide on the surface. Biochar is a kind of pyrogenic carbonaceous material that can be prepared by the thermochemical process either using physical or chemical activation at high temperatures. Biochar is very interesting to be developed as a nanocomposite that can be used as an effective adsorbent for the removal of organic and inorganic contaminations in an aqueous solution. Introducing magnetic Fe_3O_4-CuO to biochar will be a very promising material as a good selective adsorbent for the removal of inorganic anions in waste.[16] The present work aims to prepare and synthesize Fe_3O_4-CuO/biochar composite as an adsorbent. Characterization of adsorbents was observed to determine their physical and chemical properties. The efficiency of the adsorbent was applied for the removal of ion phosphate (PO_4^{3-}), nitrate (NO_3^-), nitrite (NO_2^-), and fluoride (F^-) in an aqueous solution. The adsorbent properties were investigated at different adsorption conditions in terms of pH, contact time, and concentration. The adsorption mechanism was evaluated by the Langmuir and Freundlich adsorption models and adsorption kinetic models.

EXPERIMENTAL

Materials

Palm oil shell was collected from the open areas around the palm oil industry. All chemicals such as copper(II) sulphate pentahydrate ($CuSO_4.5H_2O$), ferric chloride hexahydrate ($FeCl_3.6H_2O$), ferrous chloride tetrahydrate ($FeCl_2.4H_2O$), sodium hydroxide (NaOH), ethanol, sodium-2 (para sulphophenylazo)-dihydroxy-3,6-naphthalene desulphonated (SPANDS), N-(1-naphthyl)-ethylene diamine dihydrochloride (NEDA), sulphanilamide, hydrochloride acid (HCl), ascorbic acid, ammonium molybdate, potassium antimonial tartrate, sulfuric acid (H_2SO_4), Standard References Materials for nitrate, nitrite, phosphate, and fluoride were of analytical grade and purchased from Merck.

Characterization of Adsorbent

Characterization of adsorbent was carried out by Fourier Transform Infrared (FTIR) Spectroscopy (Perkin Elmer Spectrum Version 10.5.1), X-Ray Diffraction (XRD) method (Bruker D2 Phase Gen), the Vibration Sample Magnetometer (VSM), and Scanning Electron Microscopy with Energy dispersive X-ray (SEM-EDX) analysis (JEOL JED-2300). The Efficiency of the adsorbent for the removal of inorganic anions was calculated by UV Vis Spectrophotometry (Hitachi).

The Preparation of Biochar

The preparation of biochar was modified from the previous study.[17] Palm oil shell was washed and air-dried in sunlight for 2 days. The dried shell was crushed and sieved into granular size in 20-30 mesh. Dried granular was well impregnated with 60% phosphoric acid solution and refluxed for 24 h at 85°C. The impregnated sample was washed to reduce the chemical content and neutralized to pH 6-7 by dropping 5 M of NaOH solution, and then it was dried in an oven at 110°C for 24 h. A 100 g dried sample was put into stainless steel reactor and then placed into the graphite furnace for the pyrolysis process at 600°C for 5 h. under nitrogen gas with a flow rate of 250 cm^3min^{-1}. The yield of biochar was immersed into 3 M of HNO_3 solution and washed with distilled water to pH around 6-7. The biochar was dried in the oven at 110°C overnight and kept for the charactrization.[18,19]

Preparation of CuO Nanoparticle

The preparation of CuO was conducted by the precipitation method. Approximately, 27.802 g of $CuSO_4.5H_2O$ was dissolved in 100 ml of deionized water and strongly stirred into a homogenous solution for 1 h. The mixture was added dropwise with 3 M of NaOH solution to reach a strong base at pH 10-11. The precipitate was separated from the solution and washed with deionized water and ethanol. The yield was dried in an oven at 105ºC for 24 h.

Preparation of Fe_3O_4 nanoparticle

Preparation of Fe_3O_4 nanoparticles was carried out by precipitation method.[20] Approximately, 27.033 g of $FeCl_3.6H_2O$, and 9.942 g of $FeCl_2.4H_2O$ were dissolved in 50 ml of deionized water and strongly stirred into the homogenous solution. 3 M of NaOH solution was added into the mixture solution under vigorous stirring to pH 10-11 at room temperature. The precipitate was separated and washed with deionized water and ethanol. The sample was dried in an oven at 105ºC for 24 h. The magnetic particle of Fe_3O_4 was separated by attracting with a magnetic bar.

Synthesis of Fe_3O_4-CuO/biochar

Preparation of Fe_3O_4-CuO/biochar was carried out by hydrothermal method. About 15 g of biochar, 10 g of Fe_3O_4, and 5 g of CuO were placed into the hydrothermal reactor. The mixture was added with 50 ml of deionized water and 25 ml of ethanol. The reactor was tightly closed and slowly heated to 450 ºC for 3 h. After cooling down, the mixture was filtered, washed with deionized water, and dried at 110 ºC overnight. The result is magnetic Fe_3O_4-CuO/biochar and kept for further characterization.

Adsorption Test for Removal of Inorganic Anions

Each experiment was performed in 60 ml of each inorganic anion (nitrate, nitrite, phosphate, and fluoride). All experiment data were obtained at room temperature. The efficiency of Fe_3O_4-CuO/biochar was carried out at different adsorption parameters. The optimum pH was obtained by setting up at a concentration of 10 mg L^{-1}, adsorbent dose of 0.1 g, contact time of 30 min, and at various pH solutions (pH = 2, 4, 7, 9, and 10). The removal of ionic pollutants was conducted at different concentrations (5, 10, 15, 20, and 30 mg L^{-1}), and contact times (15, 45, 60, 90, and 120 min). The amount of solute present in the filtrate was analyzed by UV-Vis according to the procedure: nitrate (APHA 2017 4500-NO_3- B), nitrite (SNI No. 06-6989.9-2004), phosphate (SNI No. 06-6989.9-2004) and fluoride (SNI No. 06-6989.29-2005).

RESULTS AND DISCUSSION

Characterization of Fe_3O_4-CuO/Biochar

Surface Area Analysis: Fig.-1 shows the curve of nitrogen adsorption-desorption isotherm of Fe_3O_4-CuO/biochar at 77 K. Prior to analysis, the adsorbent was degassed at a temperature of 300 ºC for 8 h. The BET surface area is 263 m^2 g^{-1} obtained from the nitrogen adsorption-desorption isotherm. It was seen that the curve of adsorption isotherm sharply increased at low relative pressure and tend to plateau at higher relative pressure as an indication of Type I isotherm as the micropore structures. However, the presence of the hysteresis loop and Type IV isotherm model is the indication of the mesopore structure followed by multilayer capillary condensation.[21] This result assumed that the Fe_3O_4-CuO/biochar composite has a combination of micro and mesopore structures. However, the hysteresis curve showed unfamiliar performance with the open-ended shape line at lower relative pressure. This phenomenon may be due to incomplete combustion during the pyrolysis process. As a result, the pore of the adsorbent is easily broken or shrinkage with poor porosity. In this study, The BET surface area is higher than in previous work. This is assumed because of a higher amount concentration in the impregnation process and pyrolysis temperature.

FTIR Analysis

Fig.-2 shows the FTIR spectra of CuO, Fe_3O_4, and Fe_3O_4-CuO/biochar which are evaluated at wavenumber in the range of 4000-400 cm^{-1}. The broad bands at around 3432.82-3395.36 cm^{-1} are assigned to the O-H stretching vibrations of the hydroxyl functional group from water. The weak bands at around 1565.90-1515.21 cm^{-1} are attributed to the C=C stretching vibrations of the aromatic ring. The bands at 1441.14 and 1335.55 cm^{-1} are ascribed to the C=O and C–O stretching vibrations, respectively. The bands at around

1115.57-1062.55 cm^{-1} are assigned to the C-O stretching vibrations bound to metal cations. The presence of bands at around 874.93-765.19 cm^{-1} is attributed to the C–H group out-of-plane deformation located at the edge of the benzene derivate. The bands at 615.27-590.15 cm^{-1} can be assigned to the Cu–O and Fe–O bonds.[22,23] Some peaks of the Fe_3O_4-CuO/biochar adsorbent are missing due to the dispersion of metal oxide on the surface of biochar.

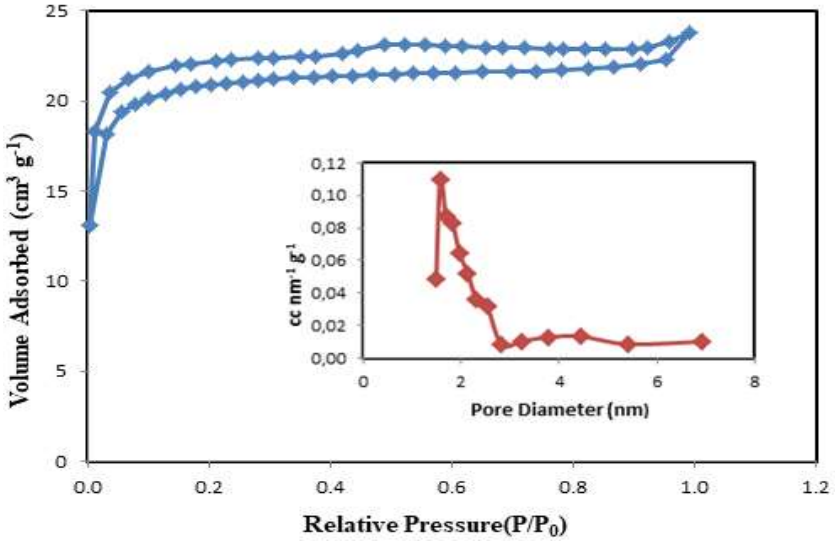

Fig.-1: Nitrogen Adsorption-Desorption Isotherm of Fe_3O_4-CuO/Biochar

XRD Analysis

Figure-3 shows the XRD diffraction pattern of CuO, Fe_3O_4, and Fe_3O_4-CuO/biochar in the range of 2θ = 10º - 80º. The CuO showed three diffraction peaks with the indexed plane at 2θ = 35.66º (111), 38.85º (111), and 48.87º (112) having a monoclinic model. This is well-matched with the previous study of JCPDS 45-0937.[24] The XRD diffraction of Fe_3O_4 showed the indexed plane 2θ = 27.41º (220), 31.77º (311), 45.50º (400), 56.33º (511), 66.29º (440), and 75.27 º (622). This result was close to a cubic spinel structure (JCPDS Card No. 019-0629). Furthermore, the Fe_3O_4-CuO/biochar showed a new peak at 31.70º (311), 35.52º (111), 38.7º (111), and 45.40º (400) compatible with Fe_3O_4 and CuO based on the previous study (JCPDS card No. 79-0419 and 89-1397).[25,26] The average crystallized size determined with the Scherrer equation is 25 nm corresponding to the nanoparticle. Comparative studies revealed that the 2θ length has changed in each material.

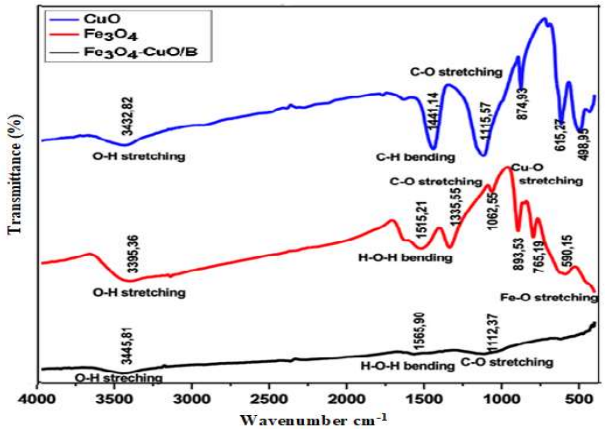

Fig.-2: The FTIR Spectra of CuO, Fe_3O_4, and Fe_3O_4-CuO/Biochar

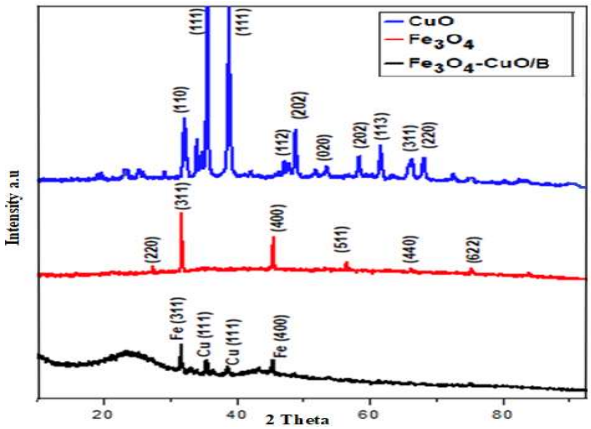

Fig.-3: XRD Pattern of CuO, Fe_3O_4, and Fe_3O_4-CuO/Biochar

The Fe_3O_4-CuO/biochar showed a significantly shifted peak as an indication of nanoparticle metal oxide that is immobilized on the surface of biochar. The crystallized size of this work is much higher compared

to the previous work.[27] In this case, the crystallized size played important roles in its application such as the performance, selectivity, and life span of the adsorbent. A higher crystallized size has more shape-selective and can accelerate the adsorption process. However, it has a lower life span by increasing its deactivation.

SEM-EDX Analysis

Fig.-4 shows the SEM microstructure of Fe_3O_4-CuO/biochar. The external surface of the adsorbent shows an irregular and rough surface texture. The surface was mostly covered by the distribution of metallic oxides of Fe-O and Cu-O. The elemental analysis and mapping spectrum of the Fe_3O_4-CuO/biochar was determined by EDX analysis. As shown in Fig.-4a shows the elemental analysis of Fe_3O_4-CuO/biochar which consist of an admixture of O, N, and S. The presence of the elements on the surface of biochar is detected from EDX mapping as shown in Fig.-4b and -4c. Each element such as iron, copper, chlorine, carbon, sulphur, nitrogen, sodium, and oxygen exhibits a specific colour. It was seen that iron and copper were on the surface of biochar. The percentage weight of carbon is much less than iron and copper. This can be concluded that the surface of biochar has been covered by metal oxides. A high concentration of chlorine was assumed from the source of chemicals of $FeCl_3$ and $FeCl_2$ during the preparation of Fe_3O_4, and sodium was from an addition of sodium hydroxide for accelerating the precipitation process. The distribution of elemental analysis can be seen from the mapping spectrum (Fig.-4b and Fig.-4c).

VSM Analysis

Figure-5 shows the vibration sample magnetometer (VSM) curve of Fe_3O_4/biochar and Fe_3O_4-CuO/biochar. The magnetic properties of the material were evaluated by the hysteresis loop curve between magnetization (M) and field (H) at room temperature. The magnetic coercivity (Hc), remanent magnetization (Mr), and saturation magnetization (Ms) were important values to determine the magnetic properties.

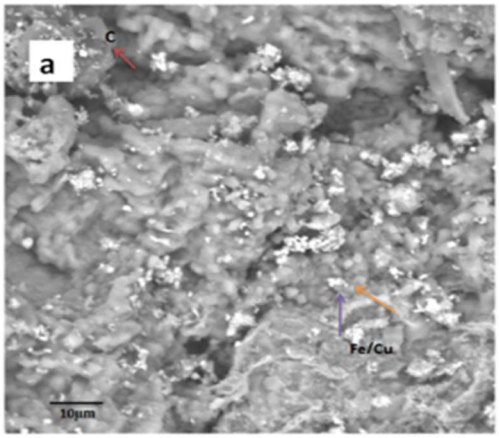

Table 1. Composition of Elements Fe_3O_4-CuO/biochar

Element Symbol	Element Name	% Weight Conc.
Fe	Iron	51.21
Cl	Chlorine	21.35
Cu	Copper	11.92
C	Carbon	7.68
O	Oxygen	6.82
Na	Sodium	0.53
S	Sulfur	0.36
N	Nitrogen	0.13
Total		**100**

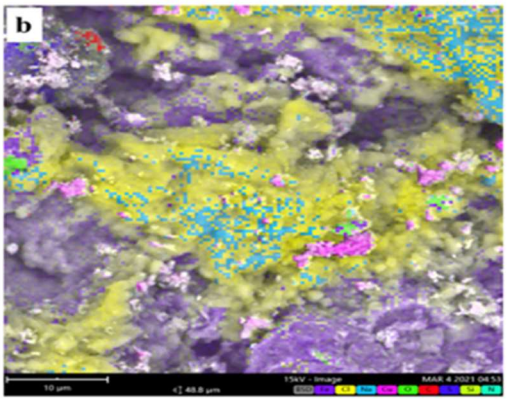

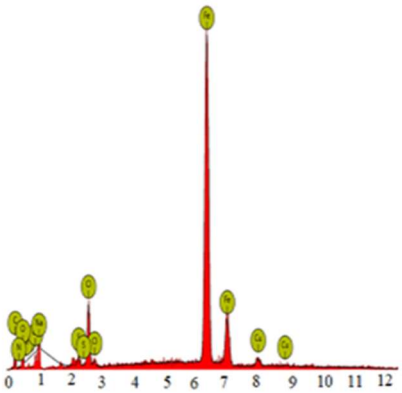

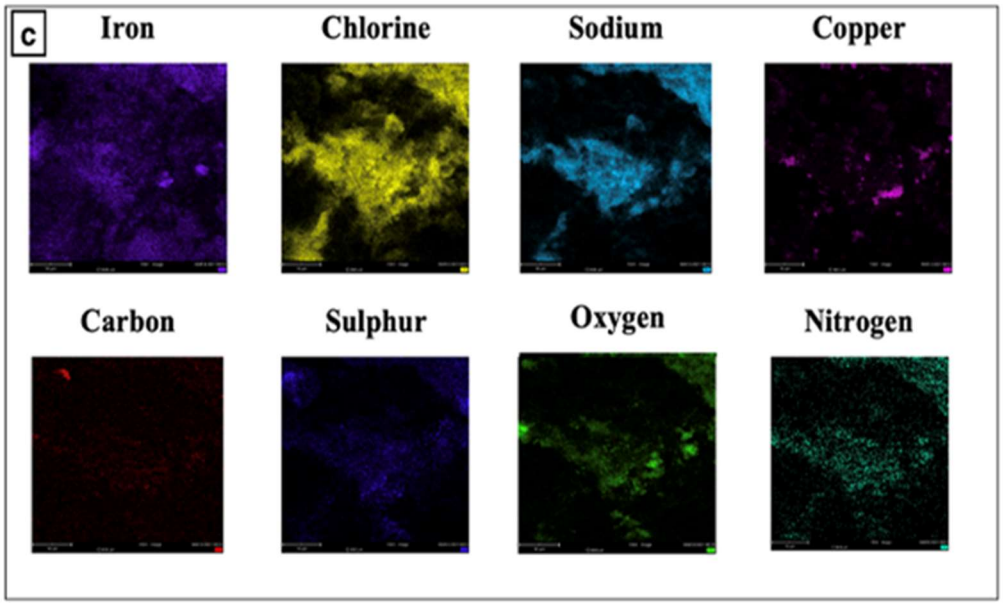

Fig.-4: SEM-EDX Analysis of a) Surface Morphology, b) Mapping of Elemental Analysis, and c) Individual Element Analysis of Fe_3O_4-CuO/Biochar

The comparison hysteresis loop shows that magnetization values were found of 40 emu/g and 1.5 emu/g for Fe_3O_4/biochar and Fe_3O_4-CuO/biochar, respectively. The effect of additional CuO has influenced the saturation magnetization. The reduction of the magnetization value of Fe_3O_4-CuO/biochar can be used as evidence that the CuO particle has bonded the magnetic Fe_3O_4 and biochar.

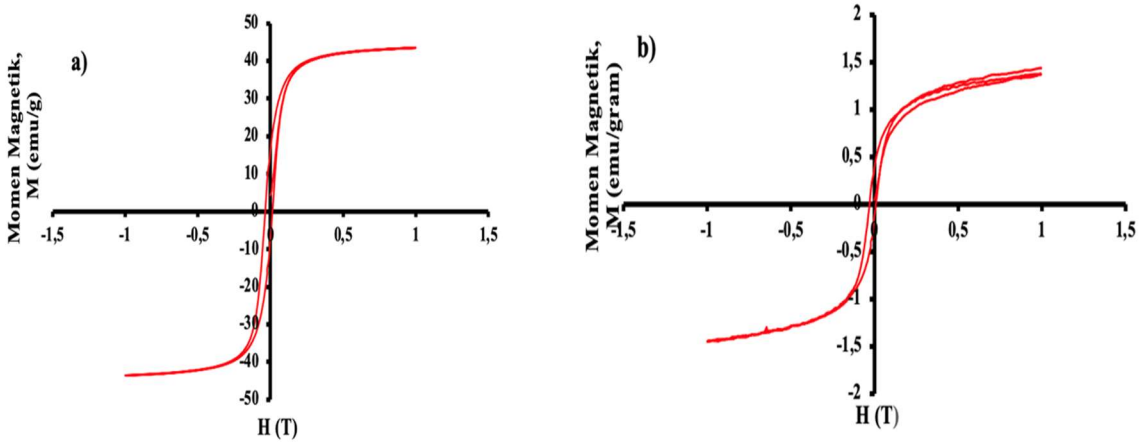

Fig.-5: VSM Analysis of (a) Fe_3O_4/Biochar and (b) Fe_3O_4-CuO/Biochar

Adsorption Application

The efficiency of magnetic Fe_3O_4-CuO/biochar was observed as an adsorbent for the removal of anions such as nitrate, nitrite, phosphate, and fluoride in water. The condition of the reaction was set up based on the different pH, contact time, and concentration. The optimum removal for a variety of applications will be obtained from the highest % adsorption value for each application with eq.1.

$$(\%)\ \text{adsorption} = \frac{(C_o - C_e)}{c_e} \text{x } 100\% \quad (1)$$

Where *Co* and *Ce* are initial anion concentration (mg L^{-1}) and anion concentration at equilibrium (mg L^{-1}), respectively.

Effect of pH

In this study, the effect of pH on the adsorption capacity of Fe_3O_4-CuO/biochar was analyzed at different pH 2, 4, 7, 9, and 10. The experiment was set up at room temperature 25 ± 3 °C, initial concentration (10 mg L^{-1}), volume (60 mL), and contact time (60 min). Fig.-6 shows the plot of the adsorption anion onto

Fe_3O_4-CuO/biochar affected by the pH solution. In general, the optimum adsorption capacity of anion was obtained in the acidic condition. The curves of nitrate and phosphate increase at the initial pH solution from 2 to 4 as optimum adsorption and then continuously decreased as the pH solution increased to 10. However, the curve of nitrite sharply decreased from pH 2 to 4 and slowly decreased to the pH solution of 10. Furthermore, the removal of fluoride tends to increase from pH 2 to pH 7 and then decrease to pH 10 with optimum adsorption at pH 7. In an acidic solution, the adsorption mechanism of anion onto Fe_3O_4-CuO/biochar showed an electrostatic attraction between the positive charge of Fe_3O_4-CuO/biochar and the negative charge of anion.[28,29] Conversely, after reaching the optimum condition, adsorption capacity decreases caused by the repulsion interaction between Fe_3O_4-CuO/biochar and anion due to the decreasing amount of positive charge of adsorbent.[30]

Effect of Contact Time

Fig.-7 shows the effect of contact time on the removal of nitrate, nitrite, phosphate, and fluoride onto Fe_3O_4-CuO/biochar. The plot of adsorption onto Fe_3O_4-CuO/biochar increases with an increase in contact times and finally reached equilibrium adsorption for nitrate at 60 min, nitrite at 90 min, phosphate at 90 min, and fluoride at 45 min. The plots tend to plateau or slightly decrease after complete sorption was achieved. This behavior occurred that the longer the contact time, the more interaction of anion and Fe_3O_4-CuO/biochar resulting in a strong attractive force between them. The decrease of adsorption capacity after reaching the equilibrium can be occurred by the repulsion of the adsorption process as saturation of electrostatic attraction between composites and anions. Furthermore, the pore of the composite has been filled full of adsorbates and repulsion of the adsorption process.[31]

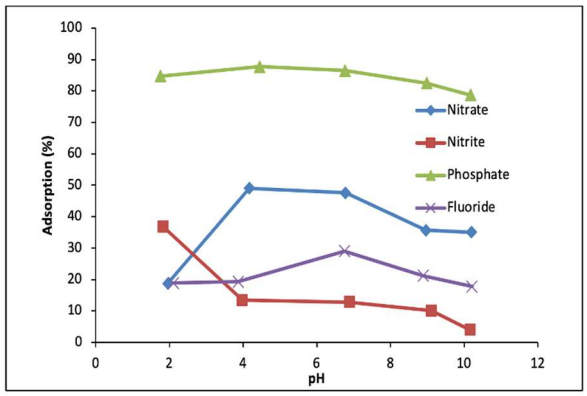

Fig.-6: Effect of pH Solution for Adsorption Anions

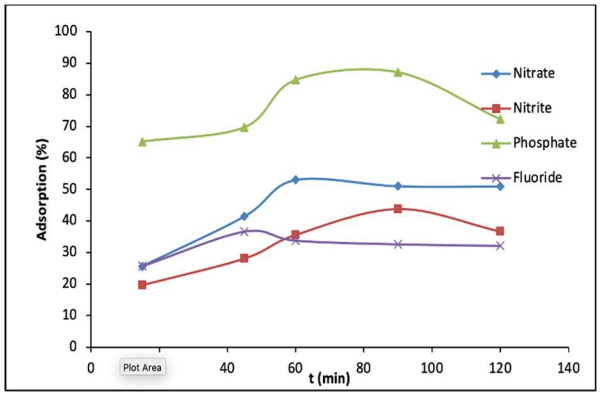

Fig.-7: Effect of Contact Time for Adsorption Anions

Effect of Concentration

Fig.-8 shows the effect of removal of nitrate, nitrite, phosphate, and fluoride onto Fe_3O_4-CuO/biochar at different concentrations of 5, 10, 15, 20, and 30 mg L^{-1}. The experiment was carried out at room temperature using the optimum pH and contact time of each anion. The results show that the trend of removal of anion onto Fe_3O_4-CuO/biochar decreased as the initial concentration increased. The highest adsorption capacity of nitrate (53.53%) and phosphate (81.65%) was achieved at the initial concentration of 10 mg L^{-1}. Furthermore, the highest adsorption capacity of nitrite (41.72%) and fluoride (50.60%) were obtained at the initial concentration of 5 mg L^{-1}. This reason can be described as that at low concertation, the anions were strongly attracted to the active site of the adsorbent. However, a higher concentration showed that the binding active site of the adsorbent became saturated and decrease the adsorption of anions. In addition, an increase in concentration is followed by decreasing in the exchangeable sites between anions and nanocomposites.

Adsorption Isotherm

Adsorption isotherm is used to describe the equilibrium reaction between adsorbate and adsorbent. To study the adsorption process of anions and onto Fe_3O_4-CuO/biochar was carried out by Langmuir and Freundlich models. The Langmuir isotherm was proposed to study the adsorption process of anions onto adsorbent

which is limited to one molecule layer. The adsorption process usually depends on the size and structure of the adsorbent system.

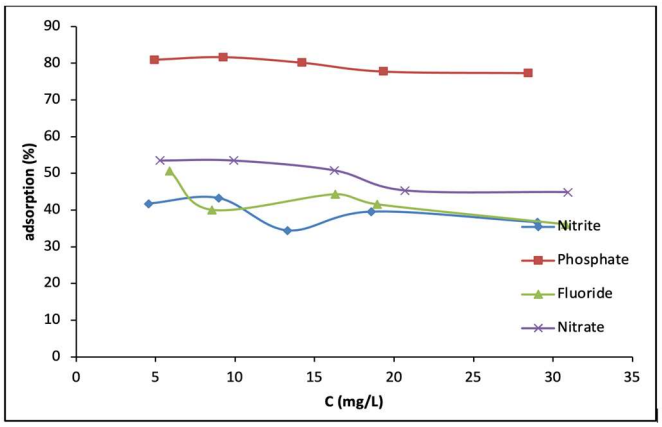

Fig.-8: Effect of Initial Concentration for Adsorption Anions

The Langmuir model of adsorption was measured from the following eq.-2.

$$\frac{1}{q_e} = \frac{1}{K_L q_m}\frac{1}{C_e} + \frac{1}{q_m} \quad (2)$$

Where C_e is the equilibrium concentration in a liquid phase (mg L^{-1}), q_e is the equilibrium adsorption capacity (mg g^{-1}), q_m is monolayer adsorption capacity (mg g^{-1}), K_L is the Langmuir constant related to the free adsorption energy (L mg^{-1}), the plot of $1/q_e$ versus $1/C_e$ should be linear and the value of K_L and q_m can be measured from the slope and intercept of the plot, respectively.

Freundlich isotherm explains the adsorption process for multilayer or heterogeneous adsorption sites. The Freundlich adsorption isotherm is expressed in its linear from the following eq. 3.

$$\log q_e = \log K_F + \frac{1}{n}\log C_e \quad (3)$$

Where K_F is a Freundlich constant indicative of the adsorption capacity (mg g^{-1}) and the constant $1/n$ relates to the intensity of the adsorption. The plot of log q_e versus log C_e should be linear and the value of K_F can be measured from the intercept and slope of the line, respectively.

The plots of the Langmuir and Freundlich isotherm models were shown in Fig.-9 and -10. It was observed that the removal of anion was well described by Langmuir and Freundlich using the value of correlation coefficient (R^2). The parameter of Langmuir and Freundlich were shown in Table 2. The Langmuir isotherm model shows that the R^2 values for adsorption of anion are closer to 1 for PO_4^{3-} ($R^2 = 0.996$), NO_3^- ($R^2 = 0.995$), NO_2^- ($R^2 = 0.978$) and F^- ($R^2 = 0.894$). It can be concluded that the anions of PO_4^{3-}, NO_3^-, NO_2^- are favorable with monolayer adsorption corresponding to the chemisorption model. However, the lowest R^2 value for the F^- can be assumed as the multilayer relating to the physisorption model. Freundlich model was the presence of the intensity of the adsorption process described by the $1/n$ values of 0.754 - 0.867. The greater the K_F value, the higher the adsorbate removal rate. The value of n represents the absorption process of the interaction between adsorbent and adsorbate. The smaller the n value, the higher the strength between the adsorbent and the adsorbate. The value of $n < 1$ indicates chemical adsorption, conversely if $n > 1$ indicates physical adsorption. The constant value of k is the level of affinity between the solution and the surface of the biochar, if the value of $K_L > 1$ then the level of affinity for biochar is strong enough. K_L value was obtained for $K_L < 1$, indicating the level of biochar's weak affinity for the adsorbate. The q_m value represents the bond between the biochar and the anion, which can form monolayer layers.[32,33]

Adsorption Kinetics

Adsorption kinetics is the rate of absorption of a fluid by the adsorbent in a certain period. The adsorption kinetics of a substance can be determined by measuring the changes in the concentration of the adsorbed substance and the value of k in the form of an intercept.[34] There is two model kinetics that is used to determine the mechanism of adsorption: the pseudo-first-order and the pseudo-second-order.

The pseudo-first-order model can be expressed as the following eq.-4.

$$\log(q_e - q_t) = \log q_e - \frac{k_1 t}{2.303} \quad (4)$$

Where q_e and q_t are the amounts of concentration adsorbed (mg g^{-1}) at the equilibrium and at any time, t (min), respectively. The k_1 (1 min^{-1}) is the rate constant of the adsorption that can be obtained from the plot of log (q_e-q_t) versus t.

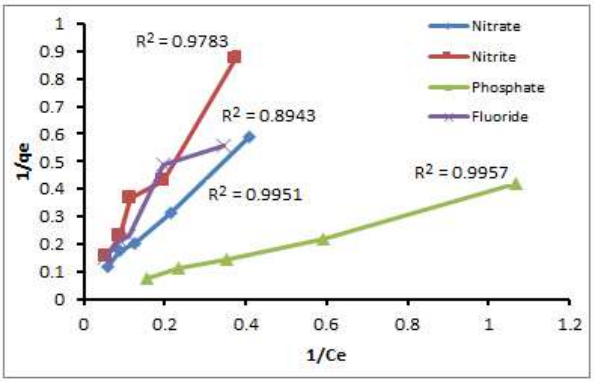

Fig.-9: Langmuir Adsorption Isotherm

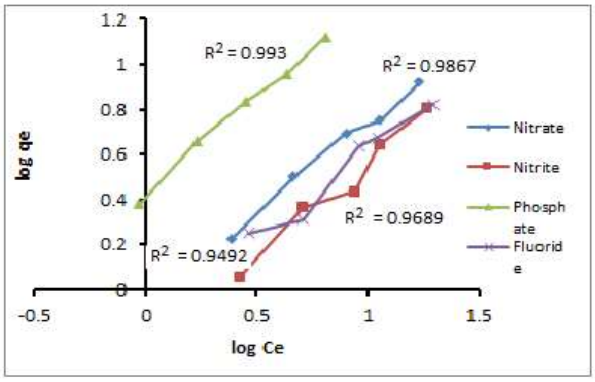

Fig.-10: Freundlich Adsorption Isotherm

Table-2. Langmuir and Freundlich Isotherm Parameters

Parameters	Nitrate	Nitrite	Phosphate	Fluoride
Langmuir				
R^2	0.9951	0.9783	0.9957	0.8943
K_L	0.0329	0.0234	0.0450	0.0628
q_m (mg g^{-1})	22.9358	19.6850	59.8800	10.7396
Freundlich				
R^2	0.9867	0.9689	0.9930	0.9492
K_F	0.8823	0.5032	2.6750	0.7349
1/n	0.7943	0.86667	0.8619	0.7536

The pseudo-second-order models can be expressed as the following eq.-5.

$$\frac{1}{q_t} = \frac{1}{k_2 q_e^2} + \frac{1}{q_e} t \quad (5)$$

Where the value of k_2 is the rate constant of Freundlich that can be determined from the linear plot of t versus t/q_t related to the value of q_t and the intercept.

Figure-11 and Table -3 show the results of the interpolation of the adsorption data of nitrate, nitrite, phosphate, and fluoride obtained from a linear plot of log (q_e-q_t) versus t (kinetic models). It can be stated that adsorption data for nitrate, nitrite, phosphate, and fluoride were not following the kinetics of the pseudo-first-order adsorption reaction because the value of the correlation coefficient (R^2) is far from unity. However, the sorption of the kinetic model tends to follow the pseudo-second-order with a fitted linearity plot ($R^2 > 0.9$).[35] The result of this investigation shows that the adsorption kinetic models show a favorable model for the pseudo-second-order.

Tabel-3: Parameters of adsorption kinetics: Pseudo-First-Order and Pseudo-Second-Order

Parameter	Nitrate	Nitrite	Phosphate	Fluoride
Pseudo-First-Order				
R^2	0.6176	0.8841	0.8301	0.8889
qe (mg/g)	0.5412	0.0668	0.4415	0.2984
k_1(1/min)	0.0136	0.0375	0.02418	0.0253
Pseudo-Second-Order				
R^2	0.9819	0.9391	0.9658	0.9928
qe (mg/g)	4.8309	2.5176	4.339	1.8822
k_2 (g/mg.min)	0.0124	0.0199	0.9716	1.7809

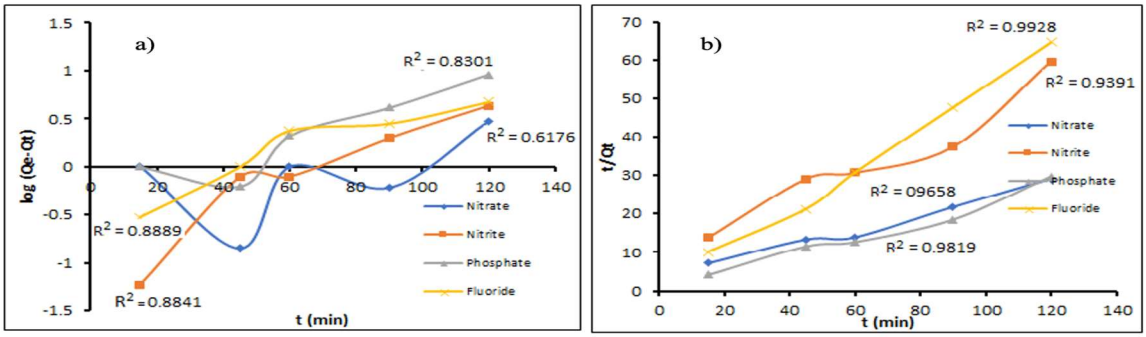

Fig.-11: Adsorption kinetics models (a) Pseudo-First-Order and (b) Pseudo-Second-Order

CONCLUSION

Magnetic Fe_3O_4-CuO/biochar nanoparticle was successfully synthesized and characterized to study their physical and chemical properties. A microstructure image shows that the adsorbent is a predominantly microporous structure based on the combination of isotherm Type I and IV. The average crystallized site of the adsorbent is about 25 nm related to the nanoparticle having a well distribution on the surface of biochar. The bonding occurring among metal, oxygen, and carbon proved that metal oxides are dispersed on the surface of biochar. The efficiency of the adsorbent was observed from the percentage removal of inorganic anions involving phosphate (PO_4^{3-}), nitrate (NO_3^-), nitrite (NO_2^-), and fluoride (F^-) at the different conditions of reactions. The maximum adsorption value of the phosphate is more than 85% found in the different pH and contact times. Anion adsorption experiment is evaluated using the Langmuir and Freundlich model. The equilibrium adsorption isotherms matched for Langmuir and Freundlich isotherm models except for the fluoride. The kinetic model shows that the pseudo-second-order is more favorable than the pseudo-first-order model. The results of this work proved the magnetic Fe_3O_4-CuO/biochar composite is a promising adsorbent to remove the inorganic anions in the aqueous solution.

ACKNOWLEDGEMENT

The authors would like to thank the Department of Chemistry, Mathematics and Natural Sciences Faculty, Universitas Islam Indonesia, and Environment Agency Yogyakarta for providing the funding and facilities to successfully perform this study.

REFERENCES

1. S. Sharma, A. Bhattacharya, *Applied Water Science,* **7**,1043(2017), https://doi.org/10.1007/s13201-016-0455-7
2. A. Tkaczyk, K. Mitrowska, A. Posyniak, *A review. Science of the Total Environment*, **717,** 137222(2020), https://doi.org/10.1016/j.scitotenv.2020.137222
3. S. Kilpimaa, H. Runtti, T. Kangas, U. Lassi, T. Kuokkanen, *Chemical Engineering Research and Design*, **92(10)**, 1923(2014), https://doi.org/10.1016/j.cherd.2014.03.019
4. A. M. E. Khalil, O. Eljamal, T. W. M. Amen, Y. Sugihara, N. Matsunaga, *Chemical Engineering Journal*, **309**, 349(2017), https://doi.org/10.1016/j.cej.2016.10.080
5. I. C. Yadav, N. L. Devi, *Data in Brief*, **28,** 104822(2020), https://doi.org/10.1016/j.dib.2019.104822
6. J. Wang, S. Wang, *Chemical Engineering Journal*, **411,** 128392(2021) https://doi.org/10.1016/j.cej.2020.128392
7. G. Tan, Y. Mao, H. Wang, N. Xu, *Chemical Engineering Research and Design*, **159**, 582(2020), https://doi.org/10.1016/j.cherd.2020.05.011
8. P. Ashokan, M. Asaithambi, V. Sivakumar, P. Sivakumar, *Rasayan Journal of Chem*istry, **15(3)**, 1596 (2022), http://doi.org/10.31788/RJC.2022.1536782
9. S. Wong, N. Ngadi, I. M. Inuwa, O. Hassan, *Journal of Cleaner Production*, **175,** 361(2018), https://doi.org/10.1016/j.jclepro.2017.12.059
10. V. H. Nguyen, H. T. Van, V. Q. Nguyen, X. Van Dam, L. P. Hoang, and L. T. Ha, *Journal of Chemistry,* **2020**, 3080612 (2020), https://doi.org/10.1155/2020/3080612
11. H. L. Huang, Z. H. Huang, Y. C. Chu, H. P. Lin, and Y. J. Chang, *Chemosphere*, **250**, 126219(2020), https://doi.org/10.1016/j.chemosphere.2020.126219

12. L. M. Tung, P. T. L. Huong, V. N. Phan, L. T. Huy, L. L. Vinh, N. Q. Hoa, H. T. Tuan, M. H. Nam, A. T. Le, *Institute of Electrical and Electronics and Engineers (IEEE) Transactions on Magnetics*, **54(6)**,(2018), https://doi.org/10.1109/TMAG.2018.2822318
13. L. R. Pereira, T. Guimarães, D. Astruc, *Coordination Chemistry Review*, **426**, 213585(2021), https://doi.org/10.1016/j.ccr.2020.213585
14. A. Q. Alorabi, H. M. Shamshi, M. Azizi, *Arabian Journal of Chemistry*, **13(11)**, 8080(2020), https://doi.org/10.1016/j.arabjc.2020.09.039
15. P. K. Singh, P. Kumar, M. Hussain, A. K. Das, G. C. Nayak, *Bulletin of Materials Science*, **39(2)**, 469(2016), https://doi.org/10.1007/s12034-016-1159-1
16. M. Zięzio, B. Charmas, K. Jedynak, M. Hawryluk, K. Kucio, *Applied Nanoscience*, **10**, 4703(2020), https://doi.org/10.1007/s13204-020-01419-6
17. A. Allwar, P. S. Septiani, P. W. Hasna, F. A. Rizky, M. Rina, R. Feby, *Institute of Electrical and Electronics and Engineers (IEEE) International Conference on Health Instrumentation &Measurement, and Natural Sciences (InHeNce)*, 978-1-6654-4181-0/2, 1, (2021)
18. P. Boguta, Z. Sokołowska, K. Skic, A. Tomzyk, *Fuel*, **256**, 115893(2019), https://doi.org/10.1016/j.fuel.2019.115893
19. K. Phiwdang, S. Suphankij, W. Mekprasart, W. Pecharapa, *Energy Procedia*, **34**,740(2013), https://doi.org/10.1016/j.egypro.2013.06.808
20. Y. Wei, B. Han, X. Hu, Y. In, X. Wang, X. Deng, *Procedia Engineering*, **27**,632(2012), https://doi.org/10.1016/j.proeng.2011.12.498
21. M.S. Ece1, A. Ekinci, S. Kutluay, O. Sahin, S. Horoz, *Journal of Materials Science: Materials in Electronics*, **32**, 18192(2021), https://doi.org/10.1007/s10854-021-06361-z
22. M. Chauhan, B. Sharma, R. Kumar, G. R. Chaudhary, A. A. Hassan, S. Kumar, *Environmental Research*, **168**, 85(2019), https://doi.org/10.1016/j.envres.2018.09.024
23. D. R. S. Cruz, B. T. J. Santos, G. C. Cunha, L. P. C. Romão, *Journal of Hazardous Materials* **334**, 76(2017), https://doi.org/10.1016/j.jhazmat.2017.03.062
24. F. Malega, I. P. T. Indrayana, E. Suharyadi, *Jurnal Ilmiah Pendidikan Fisika Al-Biruni*, **7(2)**, (2018), https://doi.org/10.24042/jipfalbiruni.v7i2.2913
25. V. M. Vinosel, S. Anand, M. S. Janifer, S. Pauline, *Materials Today Proceeding*, **8(1)**, 303(2019), https://doi.org/10.1016/j.matpr.2019.02.115
26. L. Qin, R. Ru, J. Mao, Q. Meng, Z. Fan, X. Li, G. Zhang, *Applied Catalysis B: Environmental*, **269**, 118754(2020), https://doi.org/10.1016/j.apcatb.2020.118754
27. H. Lu, L. Zhang, J. Ma, N. Alam, X. Zhou, Y. Ni, *Nanomaterials*, **9(2)**, 277(2019), https://doi.org/10.3390/nano9020277
28. M. Kamranifar, A. Naghizadeh, F. Masoudi, F. Osmani, M. Davoodi, M. R. Nabavian, *Water Science and Technology*, **82(11)**, 2250(2020), https://doi.org/10.2166/wst.2020.483
29. C. Moondeep, S. Bindu, K. Rajeev, R. C. Ganga, A. H. Ashraf, K. Sandeev, *Environmental Research*, **168**, 85(2019), https://doi.org/10.1016/j.envres.2018.09.024
30. R. R. Kalantary, E. Dehghanifard, A. Mohseni-Bandpi, L. Rezaei, A. Esrafili, B. Kakavandi, A. Azari, *Desalination and Water Treatment*, **57(35)**, 16445(2015), https://doi.org/10.1080/19443994.2015.1079251
31. A. Battas, A. E. Gaidoumi, A. Ksakas, A. Kherbeche, *The Scientific World Journal*, **2019**, 9529618(2019), https://doi.org/10.1155/2019/9529618
32. H. Nassar, A. Zyoud, A. El-Hamouz, R. Tanbour, N. Halayqa, H. S. Hilal, *Sustainable Chemistry and Pharmacy*, **18**, 100335(2020), https://doi.org/10.1016/j.scp.2020.100335
33. D. A. Almasri, N. B. Saleh, M. A. Atieh, G. McKay, S. Ahzi, *Scientific Reports*, **9**, 3232(2019), https://doi.org/10.1038/s41598-019-39035-2
34. Y.S Ho, G. McKay, *Process Biochemistry*, **34(5)**, 451(1999), https://doi.org/10.1016/S0032-9592(98)00112-5
35. R. Kh. Khamizov, *Russian Journal of Physical Chemistry* A, **94(1)**, 171(2020), https://doi.org/10.1134/S0036024420010148

[RJC-7063/2020]